ELSEVIER

Physica C 364–365 (2001) 594–599

PHYSICA C

www.elsevier.com/locate/physc

Band reflection and surface reconstruction in Sr_2RuO_4

H. Ding [a,*], S.-C. Wang [a], H.-B. Yang [a], T. Takahashi [b], J.C. Campuzano [c,d], Y. Maeno [e]

[a] *Department of Physics, Boston College, 140 Commonwealth Avenue, Chestnut Hill, MA 02467, USA*
[b] *Department of Physics, Tohoku University, 980 Sendai, Japan*
[c] *Department of Physics, University of Illinois at Chicago, Chicago, IL 60607, USA*
[d] *Materials Sciences Division, Argonne National Laboratory, Argonne, IL 60439, USA*
[e] *Department of Physics, Kyoto University, Kyoto 606-01, Japan*

Abstract

We report angle-resolved photoemission results on Sr_2RuO_4 single crystals. In addition to three Fermi surfaces which are consistent with band theory and de Haas-van Alphen result, we found the fourth band which is caused by a band folding along the (π, π) direction. This band folding is likely to be caused by a surface reconstruction.

PACS: 71.18.+y; 79.60.−i
Keywords: Ruthenate; Electronic structure; Fermi surface

The single layered ruthenate, Sr_2RuO_4 (Sr214), has generated new interest due to the recent discovery of superconductivity ($T_c \sim 1$ K) [1] and possibility of exotic (p-wave) superconducting order parameter [2–5]. In spite of a crystal structural similarity with the high temperature cuprate superconductors (isostructural to La_2CuO_4), the electronic structure of Sr214 has some major differences: it has three Fermi surfaces (FSs) with Ru $4d\epsilon(xy, yz, zx)$–O $2p\pi$ antibonding character versus a single Cu $3d_{x^2-y^2}$–O $2p\sigma$ one in cuprates. Besides differences in electronic structure, ruthenates and cuprates are different in magnetic properties. While most cuprates are close to antiferromagnetic instability, it is believed that Sr214, a Pauli paramagnet, is close to ferromagnetic instability since the cubic ruthenate $SrRuO_3$ is an itinerant ferromagnet with a Curie temperature of 150 K. However, if Sr^{2+} ions are replaced by Ca^{2+} ions, Ca_2RuO_4 is an antiferromagnetic insulator, suggesting competition between ferro- and antiferro-magnetic spin correlations. While antiferromagnetic correlation is believed to be related with the d-wave superconductivity in cuprates, it is proposed [6] that modest ferromagnetic enhancement in the Fermi liquid state of Sr214 favors a p-wave superconductivity similar to that realized in liquid ^{3}He.

ARPES has been widely used to directly measure band structure, FS and energy gap in solids. Initial ARPES measurements [7–9] in Sr214 found clear band dispersion and FS crossings, and suggested three FSs including one electron-like and

* Corresponding author. Tel.: +1-617-552-1587; fax: +1-617-552-8478.
E-mail address: dingh@bc.edu (H. Ding).

0921-4534/01/$ - see front matter
PII: S0921-4534(01)00859-0

two hole-like. The energy band for the larger hole-like FS has a flat dispersion near $(\pi, 0)$ point, or extend Van Hove singularity (VHS). These findings are not consistent with LDA band calculations [10,11] or de Haas-van Alphen (dHvA) measurement [12] which found two electron FSs and one hole FS. A recent ARPES [13] claimed that a more bulk-consistent electronic structure can be obtained at different photon energy where the VHS intensity is minimized. In this article, we report a new ARPES result based on high quality single crystals. It not only identifies all three FSs consistent with the band theory and the dHvA result, but also reveals an additional FS which is a reflection of the larger electron FS caused by the band folding of (π, π) translation. This band folding is most likely due to surface reconstruction, as observed by a recent STM study [14].

The experiments were done at the Synchrotron Radiation Center, Wisconsin, using a undulator NIM beamline. We used 22 eV photons, with a 30 meV (FWHM) energy resolution, and a momentum window of radius $0.045\pi/a$ ($a = 3.87$ Å). The Sr214 single crystals, which were grown by the traveling solvent floating zone method and annealed for more than four weeks to remove internal strains. The annealed samples have slightly enhanced T_c of 1.36 K with 0.05 K transition width. Samples are cleaved in situ in a vacuum of 10^{-11} Torr at 15 K. All cleaved samples show a mirror flat surface as evident from specular laser reflections. Samples show no sign of degradation for a period of 20 h measurement at 15 K. Samples are carefully aligned according Laue X-ray diffraction picture. High symmetric points are determined by symmetry of dispersive spectra.

Fig. 1 displays a good example of dispersive energy distribution curves (EDCs) along three major symmetric lines, Γ–M ($(0,0)$–$(\pi,0)$), M–X ($(\pi,0)$–(π,π)), and Γ–X ($(0,0)$–(π,π)) measured at 15 K. It is clear from the ARPES data, shown in lower panels of Fig. 1, that there are several energy bands and FS crossings. In order to get more quantitative description of electronic structure, it is desirable to extract band position from ARPES data. We elect the method of plotting positions of local maximum of EDCs as a function of momentum, which is the simplest way when dealing with multiple bands. The result is shown in the upper panels of Fig. 1. However, one has to be careful in associating these positions with energy bands, because some of broad spectral peaks certainly consist several bands, as evident from "shoulders" in the peaks. Nevertheless, this method gives a good description of energy states near the Fermi energy (E_F) where spectral peaks are sharp and easier to be identified individually. The fact that sharp peaks, or quasiparticle (QP) ones, appear near E_F is consistent with the Fermi liquid picture of Sr214 at low temperature [15]. We also notice that the sharp QP peaks evolve to be very broad features at higher temperature where the c-axis transport exhibits metal–insulator crossover [1,16]. This result will be described elsewhere. It is interesting to notice that the sharp QP peaks near M are almost dispersionless over a large portion of Brillouin zone (BZ). This so-called extended VHS has been observed previously [7–9]. The VHS extends along both orthogonal directions from M with the same length ($\Delta k_{flat} \approx 0.36\pi/a$), as seen in Fig. 1.

What is more significant is that spectra along Γ–X in Fig. 1 clearly reveals an opposite dispersion near $(\pi/2, \pi/2)$, that is the band moves away from E_F as momentum increases. This is totally unexpected from band theory. To identify this "unusual" band, several cuts have been measured parallel to the direction of Γ–X, as indicated in the top panel of Fig. 2. The resulting energy dispersions, using the same method described above, are plotted in lower panels of Fig. 2. It is clear from the plotted five panels of dispersion that there are three "normal" bands, which for now we label as α, β, and γ (the physical meaning of these names will become clear later in the text), as indicated in Fig. 2. It is not difficult to realize from those plots that the unusual band has a symmetric dispersion and FS crossings to the γ band with respect to the bisector line of Γ–X, which is defined by $(k_x + k_y)/2 = 0.5$ (the vertical dashed line in Fig. 2). Therefore, this unusual band, labeled as γ', is actually the "shadow" band of the real γ band caused by band folding. Band folding can be easily understood as the consequence of doubling of lattice constant, or halving of BZ. What is highly unusual of this (π, π) translation is that it only

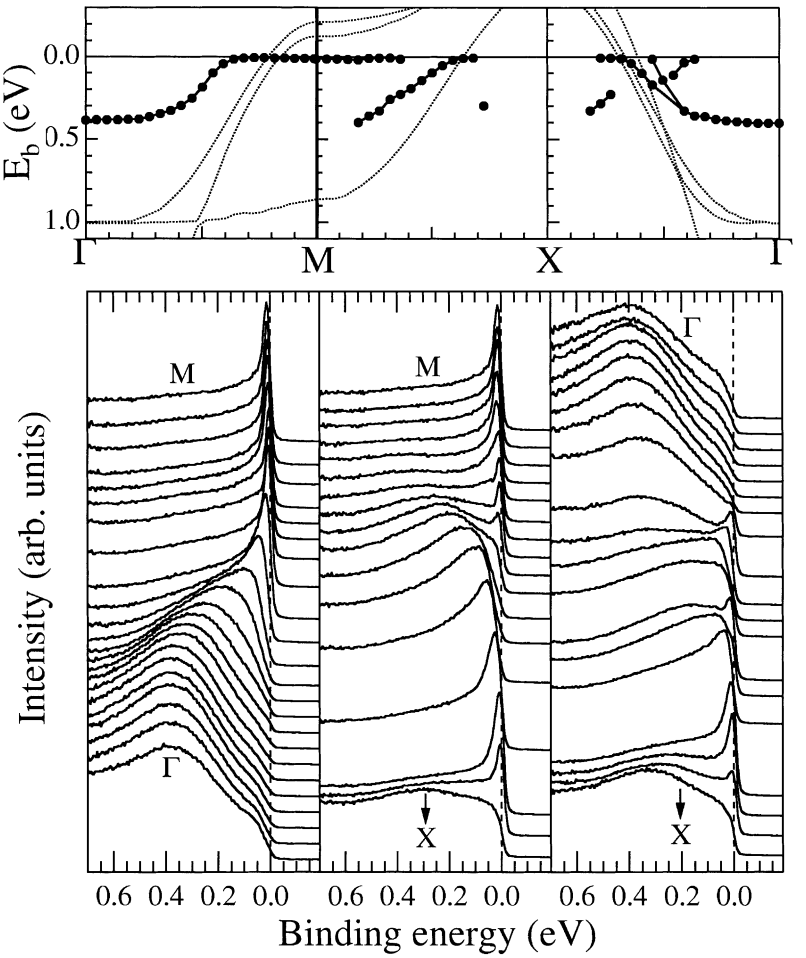

Fig. 1. Lower panels: EDCs measured at 15 K along Γ–M $((0,0)$–$(\pi,0))$, M–X $((\pi,0)$–$(\pi,\pi))$, and Γ–X $((0,0)$–$(\pi,\pi))$. Upper panels: corresponding peak position vs momentum (●), and results of band calculation $(\cdots)$ similar to the one in Ref. [10].

applies to the γ band, there is no spectral evidence of band folding for the other two bands.

To further investigate this unusual band folding, we have mapped the portion of BZ shown in Fig. 2 with a dense grid of measurement points (200 points in total) by taking advantage of high photon flux generated by the undulator and stability of sample surface. Under the symmetry of crystal, this one eighth of BZ can represent the whole zone. Fig. 3 is an image plot that integral spectral weight near E_F (from -20 to 50 meV) of EDCs is plotted in gray scale in a two-dimensional momentum space. The whole BZ plot is obtained by reflection of the original image along symmetric lines. Since the FS is defined as a contour of gapless excitations where the spectral peak passes through the E_F, this near E_F intensity plot is expected to track the FS contour closely, although the matrix element associated with photoemission may sometime distort the intrinsic representation [17]. From Fig. 3, one can identify three FSs, with two centered at Γ (electron-like) and one at X (hole-like). This is consistent with band theory [10, 11] as well as dHvA experiment [12]. For comparison, the theoretical FSs from Ref. [10] are also plotted as white dotted lines in the upper right quarter of BZ. The agreement is fairly good considering that band theory does not take account of

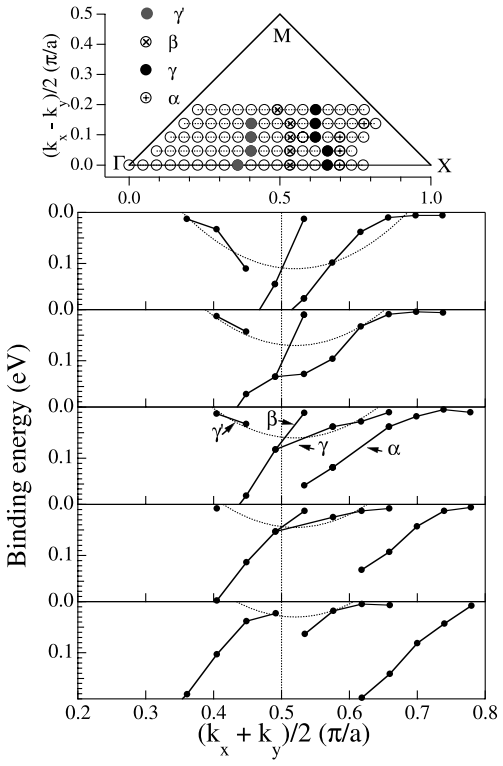

Fig. 2. Lower five panels: peak position vs momentum along cuts parallel to Γ–X, which reveals three main bands – α, β, γ, and one shadow band – γ'. Parabolic dotted lines are guides for symmetry between γ and γ' bands. Note there is slight offset of center of parabolic, $0.02\pi/a$, possibly due to a small sample misalignment (less than half a degree in real space). Upper panel: measurement points of five cuts parallel to Γ–X shown in BZ, with three main FSs – α ($\oplus$), β ($\otimes$), γ ($\bullet$), and one shadow FS – γ' ($\bullet$).

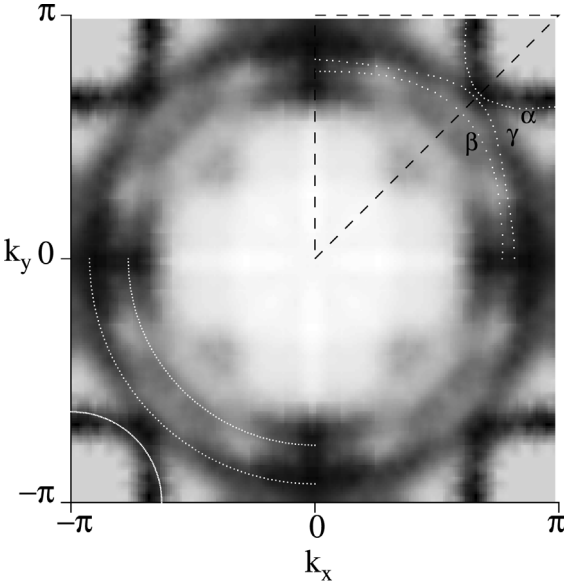

Fig. 3. Near E_F (from -20 to 50 meV) integral spectral weight plotted in the first BZ, generated by symmetry operations from the measuring grid – one eighth of BZ surrounded by the triangle. Dark region represents high integral weight. Dotted lines in upper right quarter are FSs (α, β, γ) of band calculation from Ref. [10]. Dotted lines in lower left quarter are circles with radius of average k_F from Ref. [12].

electron correlations, which are believed to be important for this system. This can be reflected by the difference of band width between ARPES experiment and the band theory, as demonstrated in the top panel of Fig. 1. The important information from the band theory is that the larger electron FS, labeled as γ, has mainly Ru $4d_{xy}$–O 2p character, while the other two FSs have hybridization of Ru $4d_{xz,yz}$–O 2p, with the electron one labeled as β and the hole one α. This is the reason for the naming convention of energy bands in Fig. 2.

To make a quantitatively comparison between results of ARPES and dHvA, we take values of average k_F obtained from dHvA measurement [12] and draw circles as approximate FSs, as plotted in lower left quarter of BZ of Fig. 3. The excellent agreement strongly suggests largely bulk representative of ARPES measurement on this material. In addition, ARPES provides detailed information of FS shape. For example, the α FS is more of a square than a circle. The sharp corner of FS may have strong influence to transport properties, like linear magnetoresistance vs field [18]. But more important finding here is that there is a shadow FS due to the folding of the γ FS, appeared as a faint and discontinuing FS arc in Fig. 3 due to much weaker intensity of the shadow band.

One of consequences of the band folding is that it makes MY and $M\Gamma$ symmetric. The equal length of flat band along these two directions is likely caused by this new symmetry. The two-dimensional extended flat band region with little dispersion makes FS near $(\pi, 0)$ ill-defined. Another possible consequence of a shadow band is that there should be an energy gap at the crossing point

of two (main and shadow) FSs due to interactions between two energy states at the same location in energy and momentum. This is indeed observed, as shown in Fig. 4a, where the leading edge midpoint shifts of EDCs along $(\pi,0)$–$(\pi/2,\pi/2)$ are plotted. In the vicinity of intersection of two FSs, the leading edge of the EDC (shown in Fig. 4b) pulls back from the E_F, with an energy gap (Δ) of 7 meV.

Having established the existence of the band folding, one will naturally ask a question – what causes it? We conclude that it most likely due to surface reconstruction as discussed below. We have performed low energy electron diffraction (LEED) measurements on the clean surface of these samples. The results show a weak c(2×2) pattern at both low (15 K) and high temperature (300 K), consistent with the measurement reported in a previous study [14]. Furthermore, a careful STM study [14] showed a clear image that the surface layer of Sr214 exhibits a strongly distorted crystal structure with RuO_6 octahedra rotated around the surface normal direction. This type of surface reconstruction is consistent with the c(2 × 2) LEED pattern and the band folding observed along the (π,π) direction.

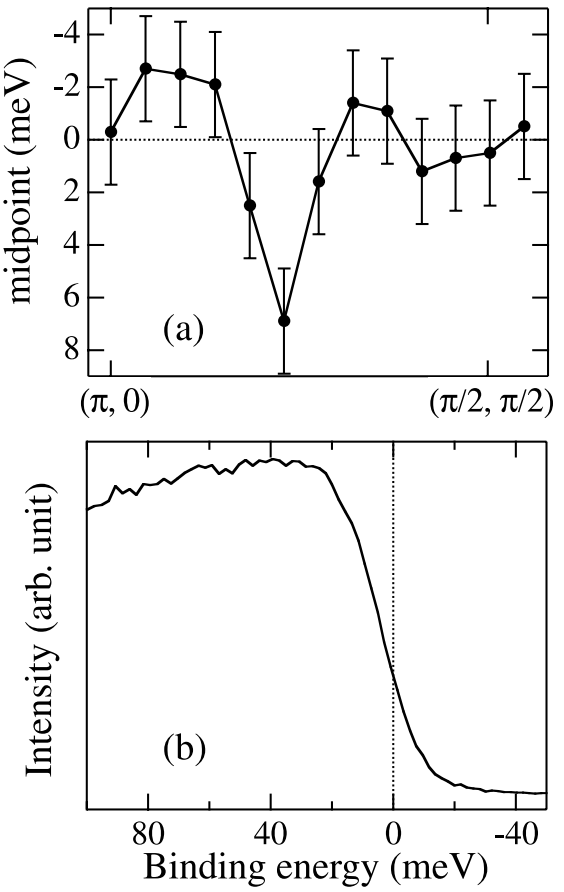

Fig. 4. (a) Midpoint shift (measured from E_F) of the leading edge of EDCs along $(\pi,0)$–$(\pi/2,\pi/2)$ direction. (b) An EDC in the vicinity of the crossing point of two bands (γ and γ'). Notice that there is a midpoint shift of 7 meV, indicating an energy gap.

The remaining mystery is that why there is only one band getting folded. In general, a simple crystalline reconstruction would affect all electron bands. One possibility is that the other two folded bands are too weak to observe due to matrix element effect. Notice that the folding band γ has mainly Ru $4d_{xy}$–O 2p character whose wave function is extended in the RuO plane. However, other possibilities exist, including possible ferromagnetic surface as suggested by some reports [14,19].

Note added: After completion of this work, we became aware of related work by Damascelli [20].

Acknowledgements

We thank Tamio Oguchi for providing band calculation results. This work was supported by the US National Science Foundation, through grant DMR-0072205, the US Dept. of Energy, the CREST of JST, and the Ministry of Education, Science, and Culture of Japan. HD is supported by a Sloan Research Fellowship. The Synchrotron Radiation Center is supported by NSF.

References

[1] Y. Maeno et al., Nature 372 (1994) 532.
[2] G.M. Luke et al., Nature 394 (1998) 558.
[3] T.M. Riseman et al., Nature 396 (1998) 242.
[4] K. Ishida et al., Nature 396 (1998) 658.
[5] T.M. Rice et al., Nature 396 (1998) 627.
[6] T.M. Rice, M. Sigrist, J. Phys.: Condens. Matter 7 (1995) L643.

[7] T. Yokoya et al., Phys. Rev. Lett. 76 (1996) 3009.
[8] T. Yokoya et al., Phys. Rev. B 54 (1996) 13311.
[9] D.H. Lu et al., Phys. Rev. Lett. 76 (1996) 4845.
[10] T. Oguchi et al., Phys. Rev. B 51 (1995) 1385.
[11] D.J. Singh et al., Phys. Rev. B 52 (1995) 13358.
[12] A.P. Mackenzie et al., Phys. Rev. Lett. 76 (1996) 3786.
[13] A.V. Puchkov et al., Phys. Rev. B 58 (1998) R13322.
[14] R. Matzdorf et al., Science 289 (2000) 746.
[15] Y. Maeno et al., J. Low Temp. Phys. 105 (1996) 1577.
[16] T. Katsufuji, M. Kasai, Y. Tokura, Phys. Rev. Lett. 76 (1996) 126.
[17] A. Bansil, M. Lindroos, J. Phys. Chem. Solids 59 (1998) 1879.
[18] R. Jin, Y. Liu, F. Lichtenberg, preprint.
[19] P.K. de Boer, R.A. de Groot, Phys. Rev. B 59 (1999) 9894.
[20] A. Damascelli et al., Phys. Rev. Lett. 85 (2000) 5194.